Journal of Solid State Chemistry 182 (2009) 3195–3200

Contents lists available at ScienceDirect

Journal of Solid State Chemistry

journal homepage: www.elsevier.com/locate/jssc

Structural studies of the phases in Ba_2LaIrO_6—New light on an old problem

Qingdi Zhou [a], Brendan J. Kennedy [a,*], Maxim Avdeev [b], Lisa Giachini [c], Justin A. Kimpton [c]

[a] School of Chemistry, The University of Sydney, Sydney, NSW 2006 Australia
[b] Bragg Institute, Australian Nuclear Science and Technology Organisation, Private Mail Bag 1, Menai NSW 2234, USA
[c] Australian Synchrotron, 800 Blackburn Rd, Clayton, Victoria 3168, Australia

ARTICLE INFO

Article history:
Received 23 June 2009
Received in revised form
18 August 2009
Accepted 23 August 2009
Available online 4 September 2009

Keywords:
Perovskite
Iridium oxide
Phase transition

ABSTRACT

Accurate and precise structures for the cation-ordered double perovskite Ba_2LaIrO_6 at a number of temperatures are presented. Careful analysis of the synchrotron X-ray and neutron diffraction profiles of Ba_2LaIrO_6 suggests that, at room temperature, this is monoclinic in space group $I2/m$. Heating the sample to 375 K results in a transition to a rhombohedral phase in $R\bar{3}$ with further heating resulting in the loss of the tilting of the octahedra, the structure being in $Fm\bar{3}m$. Cooling the sample induces an additional phase transition to a triclinic structure in $I\bar{1}$. Details of the various structures are presented.

1. Introduction

For well over half a century the structural chemistry, electronic and magnetic properties of ABO_3 perovskites including the $A_2BB'O_6$ double perovskites, in which two different ions are regularly ordered at the octahedral *B*-site, have been of interest [1–3]. The enormous flexibility of perovskites allows the possibility of forming materials with highly tailored compositions, and hence structures and ultimately properties. The solid-state chemistry of mixed-metal oxides containing ruthenium or iridium has attracted a great deal of recent research reflecting the diverse range of structures and electronic properties displayed by such oxides [4]. For example, the perovskite $SrRuO_3$ is ferromagnetic below 160 K [5] and the layered perovskite Sr_2RuO_4 is a superconductor below 1 K [6].

Despite the strong correlation between structure and properties in perovskites, accurate and precise structures of numerous well studied examples are not available. Ba_2LaIrO_6 is a case at point. This oxide was apparently first prepared by Thumm et al. [7] who concluded that it was cubic with ordering of the La and Ir cations. Ramos et al. [8] reported the material was actually orthorhombic without ordering of the La and Ir cations. In 1999 Wakeshima et al. [9] also reported ordering of the cations but suggested the true symmetry was monoclinic in $P2_1/n$. Most recently Fu and Ijdo [10] concluded the symmetry was actually rhombohedral in space group $R\bar{3}$; both this and $P2_1/n$ allow ordering of the two *B*-site cations. Whilst differences in preparative methods occasionally result in different symmetries, it is more common that the high pseudo-symmetry and weakness of selected diagnostic reflections leads to uncertainty in the choice of space group. This is especially true when the structures are determined by powder X-ray diffraction methods utilizing non-monochromatic Cu radiation on laboratory-based diffractometers as employed in the above four experimental studies. Xiang et al. [11] concluded from density functional theory calculations that the most likely structure of Ba_2LaIrO_6 was rhombohedral.

The continuing interest in Ba_2LaIrO_6 prompted us to re-examine the structure of this oxide using both synchrotron X-ray and neutron powder diffraction.

2. Experimental

Samples of Ba_2LaIrO_6 and La_2ZnIrO_6 were prepared by solid-state reaction from stoichiometric mixtures of high purity $BaCO_3$, La_2O_3, ZnO and Ir. After mixing, the powders were placed in alumina crucibles and calcined at 900 °C overnight before been heated at 1200 °C for 6 days with periodic regrinding of the mixture. After the final heating the samples were slowly cooled to around 100 °C before being removed from the furnace. The reactions were continued until powder X-ray diffraction patterns, collected using a Shamdzu D6000 diffractometer, no longer changed.

Ir L_3-edge X-ray absorption spectroscopic measurements were carried out at BL-12 of the Australian Synchrotron, Melbourne, Australia [12]. The beamline has a 1.9 T wiggler as its source, a bendable collimating mirror, Si(1 1 1) liquid nitrogen cooled fixed offset double crystal monochromator and a dual toroid refocusing

* Corresponding author.
E-mail address: B.Kennedy@chem.usyd.edu.au (B.J. Kennedy).

0022-4596/$ - see front matter © 2009 Elsevier Inc. All rights reserved.
doi:10.1016/j.jssc.2009.08.026

mirror. For measurements at the Ir L_3-edge Rh stripes were used in both mirrors. Room-temperature spectra were recorded in transmission mode. The photon flux was of the order of 5×10^{10} photons/s and the spot size around 1 (h) × 0.5 (v) mm. Data points were collected with energy steps of 0.25 eV. The monochromator energy scale was calibrated to the L_3-edge of Au metal foil (first inflection point assigned to 11,919 eV).

The synchrotron X-ray diffraction data were collected using the MYTHEN microstrip detector on the powder diffractometer at BL-10 of the Australian Synchrotron [13]. The samples were housed in 0.2 mm diameter capillaries that were rotated during the measurements. Data were recorded at ambient temperature in the angular range $5<2\theta<85^\circ$, using X-rays of wavelength 0.82667 Å as estimated using NIST LaB_6 (SRM 660a). Data at temperatures above room temperature were obtained at the same beamline using 0.63700 Å X-rays. Neutron powder diffraction data of the samples were measured using the high-resolution powder diffractometer Echidna at ANSTO's OPAL facility at Lucas Heights [14] using wavelengths of 1.622 or 2.439 Å. For these measurements the sample was contained in a cylindrical vanadium can. The structures were refined using the program RIETICA [15]. For neutron diffraction patterns, the background was calculated using a six-parameter polynomial while for the X-ray patterns, the background was estimated by interpolating between up to 40 selected points. The effects of absorption were modeled in refinements using both X-ray and neutron data sets.

3. Results and discussion

The valence states of the Ir cations in the $Ba2LaIrO_6$ and La_2ZnIrO_6 were probed by examining the Ir L_3-edge using X-ray absorption Near Edge Structure (XANES) spectroscopy. The Ir L_3 line of Ba_2LaIrO_6 is characterised by a poorly resolved doublet corresponding to the transition from Ir 2p to 5d orbitals, where separate transitions to the t_{2g} and e_g orbitals are evident. By comparison the Ir L_3-edge spectrum of the Ir^{4+} oxide La_2ZnIrO_6 appears as a singlet, due to smaller separation of the two peaks and lower intensity in the t_{2g}-related peak. The Ir L_3-edge appears at higher energy (by ~1.5 eV) in Ba_2LaIrO_6 than it does in La_2ZnIrO_6. These observations are consistent with the Ir being present as Ir^{4+} in La_2ZnIrO_6 and Ir^{5+} in Ba_2LaIrO_6 [16] (Fig. 1).

Before describing the results of our diffraction studies it is appropriate to comment on the basis of our space group choices.

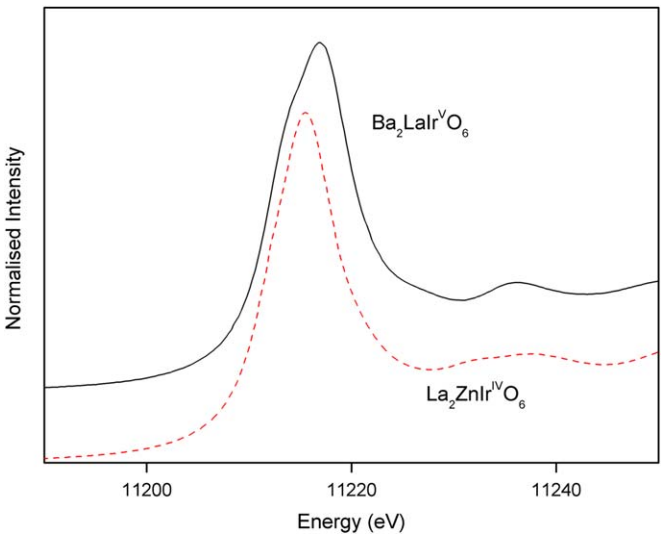

Fig. 1. Observed Ir L_3 spectra for $La_2ZnIr^{IV}O_6$ and $Ba_2LaIr^{V}O_6$.

Establishing the precise structure of the double perovskites using X-ray powder diffraction often presents a number of challenges. The rock-salt like ordering of the two B-site cations in $A_2BB'O_6$ perovskites results in a doubling of the primitive cell associated with a R_1^+ ($\boldsymbol{k}=\frac{1}{2}\frac{1}{2}\frac{1}{2}$) mode [17]. This allows for a number of additional reflections with *odd–odd–odd* indices in the diffraction patterns, over that seen in the pattern of archetypal cubic $Pm\bar{3}m$ ABO_3 perovskites. Such additional reflections are commonly described as R-point superlattice reflections. The intensity of these is dependent on the difference in scattering power between the two B-site cations. Relatively few perovskites have a cubic structure, with lower symmetries often observed due to a mismatch in size between the A- and B-type cations resulting in cooperative tilting of the BO_6 octahedra. Howard et al. [17] have used group theory to identify possible space groups and the relationships between these for the rock-salt-like ordered $A_2BB'O_6$ perovskites.

Out-of-phase tilting of the BO_6 octahedra in double perovskites is associated with a R_4^+ ($\boldsymbol{k}=\frac{1}{2}\frac{1}{2}\frac{1}{2}$), mode. This permits the same R-point reflections as does the B-site cation ordering. The intensity of the R-point reflections, due to octahedral tilting, is dependent on the magnitude of the displacement of the oxygen anions. In the presence of heavy cations such as Ba, La and Ir the octahedral tilting will contribute very little to the X-ray intensity of the R-point superlattice reflections, especially where there is an appreciable difference in the scattering power of the two ordered B-site cations as occurs, for example, in Ba_2LaIrO_6. Conversely in neutron diffraction the majority of the intensity of the R-point reflections may arise from the magnitude of the out-of-phase tilts. Indeed it is possible that the difference in neutron scattering lengths of the two B-type cations may be insignificantly small so as not to appreciably contribute to the R-point reflections. Examination of Howard et al. [17] identifies 12 possible space groups for double perovskites and of these five will only display R-point superlattice reflections, in addition to the parent Bragg reflections.

In-phase tilting in the double perovskites is described by a M_3^+, ($\boldsymbol{k}=\frac{1}{2}\frac{1}{2}0$), mode. This produces superlattice reflections with *even–odd–odd* indices. The simultaneous occurrence of M-point and R-point distortions will produce some X-point reflections, indexing as *even–even–odd*. Such X-point reflections are usually very weak in perovskites, such as $CaMnO_3$ [18] or $CaTiO_3$ [19], however provided the scattering difference between the two B-site ordered cations is sufficiently large significant X-ray intensities at the X-points may be observed. If neutron, rather than X-ray, diffraction is employed then the magnitude of the M-point reflections due to the tilting of the octahedra is expected to be somewhat stronger.

Of course, lowering the symmetry from cubic will also result in splitting of some of the stronger main Bragg reflections. In the case where only R-point reflections are observed the possible space groups and corresponding Glazer tilt systems are $Fm\bar{3}m$ ($a^0a^0a^0$), $I4/m$ ($a^0a^0c^-$), $R\bar{3}$ ($a^-a^-a^-$) and $I2/m$ ($a^0b^-b^-$). There is also the possibility of a triclinic cell in $I\bar{1}$ ($a^-b^-c^-$). These possibilities can, in principle, be distinguished by examining the splitting of selected diagnostic reflections, assuming there is no accidental degeneracy. The parent (2 2 2) reflection, that occurs near d=1.15 Å for a perovskite in $Pm\bar{3}m$ with a=4.0 Å, appearing as a singlet in $Fm\bar{3}m$ and $I4/m$ but can be split in both $I2/m$ and $R\bar{3}$. In the former case a triplet with an intensity ratio of 1:1:2 is expected, although if the monoclinic angle in near 90° this may be a doublet. In the latter case the (2 2 2) reflection should be a doublet with an intensity ratio of 3:1. The (4 0 0) reflection is unsplit in $Fm\bar{3}m$ and $R\bar{3}$ but splits in $I4/m$ and $I2/m$. Both the 2 2 2 and 4 0 0 reflections can split in $I\bar{1}$. Once the appropriate space group is identified then the validity of this can be assessed by Rietveld refinement, although we stress that structure

refinements should not be used to identify possible structures. In the case where both *M*- and *X*-point reflections are observed, in addition to the *R*-point reflections associated with the cation ordering and in-phase tilts, the cell metric is used to distinguish between the possible space groups.

The above discussion seems to imply that establishing the appropriate space groups should be straightforward but in practice incorrect assignments are common. This is due to the weakness of many of the diagnostic superlattice reflections, coupled with the modest peak shape resolution of many powder diffractometers and also the pathological tendency of perovskites to display pseudo-symmetry. Considering La_2ZnIrO_6 as an example, the synchrotron X-ray diffraction pattern is illustrated in Fig. 2. This data shows the presence of *R*-, *M*- and *X*-point reflections in addition to splitting of both the $(2\,2\,2)_p$ and $(4\,0\,0)_p$ reflections. As evident from Fig. 2 the data was well fit in the monoclinic space group $P2_1/n$ ($a^-a^-c^+$) as originally proposed by Currie et al. [20] and Battle and Gore [21]. The validity of this model was verified by successful Rietveld refinement using a powder neutron diffraction data set. The final refined structural parameters together with selected bond distances are available as supplementary data.

Turning now to Ba_2LaIrO_6, the synchrotron and neutron diffraction data (Fig. 3) show only *R*-point reflections eliminating the postulate by Wakeshima et al. [9] of $P2_1/n$. Based on the observed strength of the *R*-point reflections in the XRD pattern, the unordered orthorhombic model proposed by Ramos et al. [8] is also discarded. The synchrotron pattern shows well-resolved splitting of the $(2\,2\,2)_p$ (near $2\theta=39^\circ$) but not the $(4\,0\,0)_p$ near $2\theta=45.5^\circ$ reflections, consistent with $R\bar{3}$ described by Fu [10]. Attempts to refine a structure in $R\bar{3}$ against the synchrotron XRD data were, however, unsuccessful, in particular the fit to the $(3\,2\,1)_p$ reflection near $2\theta=42.5^\circ$ was less than optimal and the various measures of fit were higher than anticipated, e.g. $\chi^2=20.4\%$. Nor did this model adequately fit the neutron diffraction pattern. It appears that there is a further lowering of symmetry. We then considered a model in $I2/m$ and although this provided a satisfactory fit to the neutron data and improved the fit to the X-ray data ($\chi^2=14.3\%$) it failed to model the observed shape of some reflections. Previously Battle has proposed the use of a triclinic model in $I\bar{1}$ for some ordered double perovskites, including the closely related oxide Ba_2LaRuO_6 [22], however this model also failed to give acceptable refinements ($\chi^2=12.3\%$) (Fig. 4).

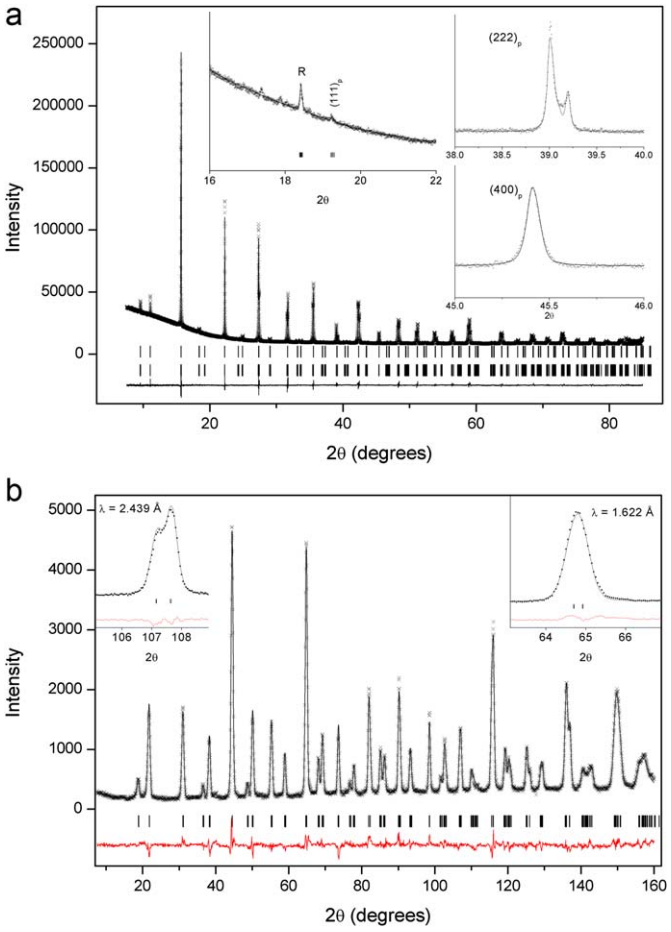

Fig. 3. (a) Synchrotron X-ray diffraction profiles for Ba_2LaIrO_6 recorded at room temperature. The insets highlight the presence of the diagnostic superlattice reflections and splitting of the Bragg reflections. The upper set of reflection markers are for the monoclinic $I2/m$ phase and the lower set for the rhombohedral $R\bar{3}$ phase. The two unindexed peaks near 17° in the inset have an intensity of $<0.05\%$ that of the strongest Bragg reflection. (b) Neutron profiles fitted in $I2/m$. The data was collected at 1.622 Å. The insets show splitting of the 2 2 0 reflection apparent when a longer wavelength was used to collect the data.

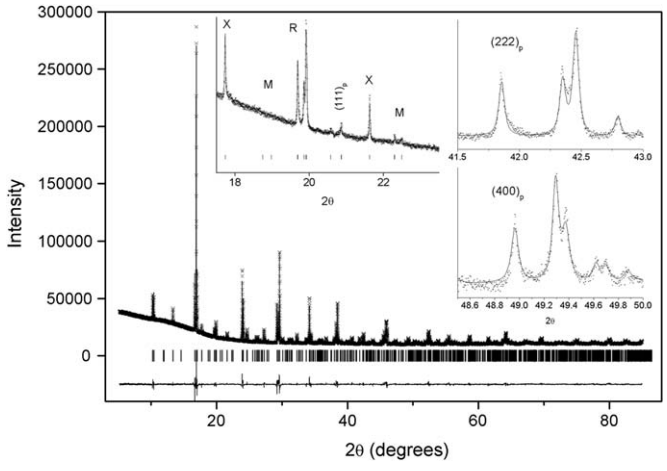

Fig. 2. Synchrotron X-ray diffraction profiles for La_2ZnIrO_6 recorded at room temperature. The insets highlight the presence of the diagnostic superlattice reflections and splitting of the Bragg reflections.

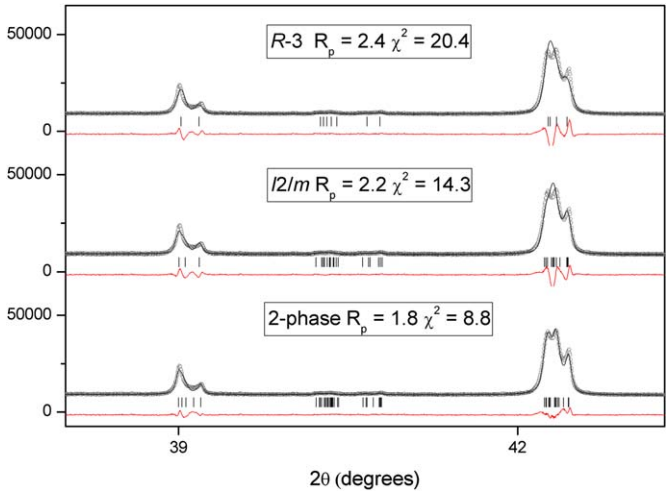

Fig. 4. Portions of the room temperature Rietveld X-ray diffraction profiles illustrating the splitting of the 2 2 2 near $2\theta=39^\circ$ and 3 2 1 near $2\theta=42.5^\circ$ reflections. The latter is only adequately fitted using a mixture of $I2/m$ and $R\bar{3}$.

Finally we considered the possibility that the sample contains a mixture of both $I2/m$ and $R\bar{3}$. In double perovskites the transition between these two structures must be first order and, as recently described by Saines et al. [23] and Fu et al for Ba_2SrWO_6 [24], on occasions these two phases can co-exist. Using a two phase $I2/m$ and $R\bar{3}$ model we obtained an excellent fit to the room temperature synchrotron diffraction data (χ^2=8.8%), although the amount of rhombohedral phase present was estimated to be less than 10 wt% in the Rietveld analysis. The volume of the rhombohedral phase is slightly smaller than that of the monoclinic phase. Heating the sample to above 373 K simplified the appearance of the $(3\,2\,1)_p$ reflection and it was possible to obtain good fits to the synchrotron diffraction data using a single phase $R\bar{3}$ rhombohedral model. Heating to still higher temperatures resulted in further simplification of the patterns and there was no indication of any peak splitting or broadening in the patterns recorded at or above 473 K demonstrating $Fm\bar{3}m$ to be appropriate. The temperature dependence of the rhombohedral angle, α, for the patterns recorded between 348 and 473 K is illustrated in Fig. 5 and demonstrates a continuous $R\bar{3} \rightarrow Fm\bar{3}m$ transition. This sequence of transitions is consistent with the group theoretical analysis of Howard et al. [17].

Powder neutron diffraction data was collected for an, independently prepared, sample of Ba_2LaIrO_6, to obtain accurate and precise structural parameters for this oxide. As a consequence of the lower peak shape resolution of this data, compared to the synchrotron data, it was possible to fit the pattern recorded at RT to a single phase model in $I2/m$ with χ^2=2.46. Fitting this data to a model in $R\bar{3}$ gave a noticeably poorer fit, χ^2=4.26. We note that the neutron pattern obtained at λ=2.439 Å showed clear splitting of selected Bragg reflections, that was not observed in the data recorded at 1.622 Å, see Fig. 3. The longer wavelength data demonstrates the structure cannot be rhombohedral at room temperature. The structural parameters reported for Ba_2LaIrO_6 at room temperature are based on a refinement using both data sets. Attempts to implement the two phase $I2/m$ and $R\bar{3}$ model did not result in a stable refinement against the RT patterns, possibly reflecting the lower resolution of the neutron diffractometers. Upon cooling the sample remained monoclinic to at least 200 K. Further cooling resulted in obvious changes to the appearance of the pattern but critically there were no M- or X-point reflections in any of the neutron diffraction patterns, see Fig. 6. Clearly cooling did not introduce a transition to $P2_1/n$, rather the structure became triclinic. Since only R-point superlattice reflections were observed we fitted the data using a model in $I\bar{1}$. The structural parameters for the four phases of Ba_2LaIrO_6 observed in this work are summarized in Table 1.

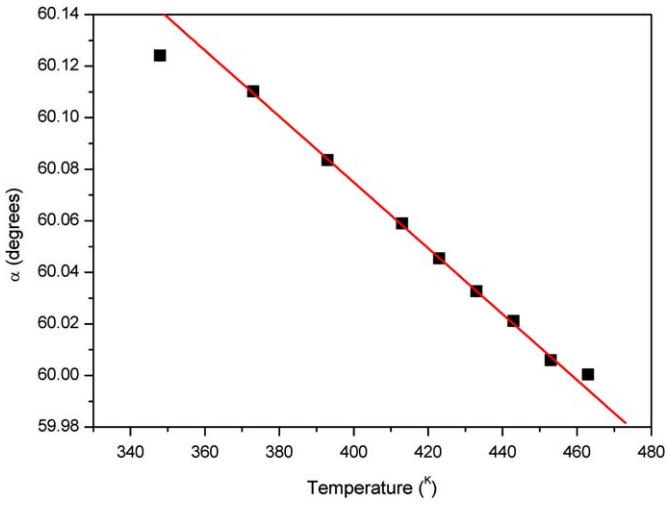

Fig. 5. Temperature dependence of the unique angle in the rhombohedral phase of Ba_2LaIrO_6. A linear fit to the data demonstrates this to be continuous. A small amount of the monoclinic phase is evident in the data recorded at 75° resulting in the anomalous value.

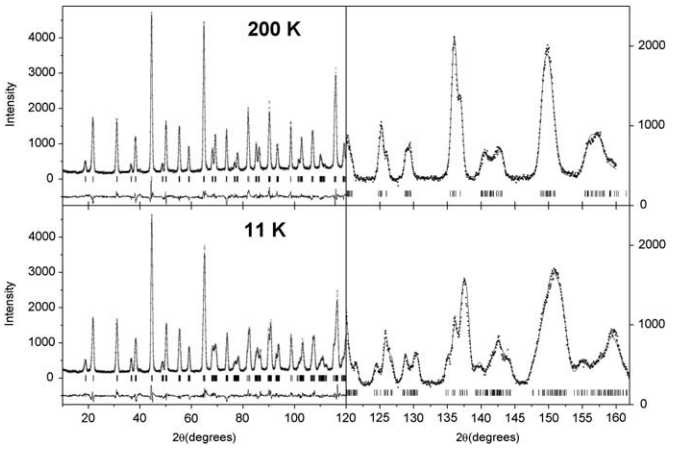

Fig. 6. Rietveld plot of the neutron (1.622 Å) data for Ba_2LaIrO_6 at 2 0 0 and 11 K illustrating the transition from $I2/m$ at 200 K to $I\bar{1}$ at 11 K. *Note the change in scale near* 2θ=120° used to highlight the differences.

Although the room temperature synchrotron diffraction X-ray pattern for Ba_2LaIrO_6 suggests, based on the observed superlattice reflections and peak splitting, this is rhombohedral, profile fitting indicates the sample studied is actually monoclinic in $I2/m$. This conclusion was confirmed using neutron diffraction. Heating Ba_2LaIrO_6 to 375 K induces a transition to a pure rhombohedral phase in $R\bar{3}$, with further heating to above 463 K causing a transition to $Fm\bar{3}m$. The transition temperature was estimated from analysis of the temperature dependence of the rhombohedral angle. The temperature dependence of the rhombohedral angle demonstrates this transition to be continuous as allowed by group theory.

The average Ir–O distance in the room temperature structure of Ba_2LaIrO_6, 1.988 Å, was noticeably shorter than that found in various Ir^{4+} oxides including IrO_2 [25] and La_2ZnIrO_6 (Table S1) as expected for Ir^{5+} compared to Ir^{4+}. A similar reduction is seen in the two oxides $Sr_2Tb^{4+}Ir^{4+}O_6$ Ir–O_{av} 2.017 Å and $Ba_2Tb^{3+}Ir^{5+}O_6$ Ir–O_{av}=1.970 Å [26]. The change in iridium valence state in the two present oxides was verified by X-ray absorption spectroscopy. The corresponding BVS was 5.33. The average bond length for the La^{3+} octahedron is unexceptional 2.313 Å, although the BVS, 4.12, is somewhat greater than expected, suggesting either the tabulated constants are inappropriate or there is some local strain in the M–O bonds [27]. We have calculated the BVS for the La cation in Ba_2LaRuO_6 using the published bond distances [10] and find that is comparable to that found here, 4.3. Whilst the average Ir–O bond distance in this oxide was unexceptional the anisotropy of the Ir–O bonds lengths is not. As evident from Table 1 the two axial Ir–O bonds are noticeably shorter than the four equatorial bonds 1.924(4) vs 2.009(6) Å. Distortion of the octahedra in ordered double perovskites have been observed previously, reflecting the different bonding requirements of the various cations. However the distortion of the IrO_6 octahedra is greater than that observed in $Ba_2Bi^{III}Bi^{V}O_6$ [28] and Ba_2NdNbO_6 [29,30], two other well characterised monoclinic double perovskites, but it is comparable to that reported for Ba_2SrWO_6 [31] which also adopts $I2/m$. Whilst it is possible that the distortion is a consequence of an electronic effect as observed in some Jahn–Teller distorted perovskites such as $LaMnO_3$ [32] or Ba_2CuUO_6

Table 1
Structural Parameters and selected bond distances for Ba_2LaIrO_6.

T (K)	11	295	423	473
Space group	$I\bar{1}$	$I2/m$	$R\bar{3}$	$Fm\bar{3}m$
a (Å)	6.0480(2)	6.0481(3)	6.07440(4)	8.5986(1)
b (Å)	6.0387(2)	6.0664(3)	a	a
c (Å)	8.5655(4)	8.5634(5)	a	a
α (deg)	89.843(3)	90	60.045(1)	90
β (deg)	90.653(2)	90.256(3)		90
γ (deg)	90.200(4)	90		90
Ba				
x	0.5029(9)	0.5007(9)	0.2512(2)	$\frac{1}{4}$
y	0.4939(11)	0	x	$\frac{1}{4}$
z	0.2495(7)	0.2568(8)	x	$\frac{1}{4}$
B_{iso}	0.46(3)	1.05(3)	1.17(1)	1.44(1)
La				
B_{iso}	0.59(3)	1.10(4)	0.56(1)	0.78(1)
Ir				
B_{iso}	0.75(3)	0.54(3)	0.59(1)	0.64(1)
O(1)				
x	0.2958(9)	0.0082(12)	0.2396(12)	0.2715(5)
y	0.2530(14)	0	0.3066(12)	0
z	0.9959(6)	0.2754(5)	0.7238(21)	0
B_{iso}	0.86(10)	1.73(11)	0.82(12)	2.78(9)
O(2)				
x	0.2486(8)	0.2822(5)		
y	0.7939(10)	0.2519(9)		
z	0.0256(8)	−0.0227(4)		
B_{iso}	1.23(6)	1.58(6)		
O(3)				
x	0.5222(10)			
y	0.0282(11)			
z	0.2275(8)			
B_{iso}	0.52(8)			
La–O(1) (Å)	2.334(6) × 2	2.358(4) × 2	2.356(10) × 6	2.335(4) × 6
La–O(2) (Å)	2.331(7) × 2	2.230(5) × 4		
La–O(3) (Å)	2.345(7) × 2			
Ir–O(1) (Å)	1.968(7) × 2	1.924(4) × 2	1.960(10) × 6	1.965(4) × 6
Ir–O(2) (Å)	1.975(6) × 2	2.009(6) × 4		
Ir–O(3) (Å)	1.960(7) × 2			

The structures at 11 and 295 K were refined using neutron diffraction data, and those at 423 and 473 K synchrotron X-ray data. The 295 K refinement employed two neutron data sets recorded at 1.622 and 2.439 Å, whereas the 11 K used a single data set recorded at 1.622 Å. In all cases the La and Ir are on special positions, In $I\bar{1}$ La is at $0\frac{1}{2}0$ Ir $\frac{1}{2}00$. In all other cases the La cations are at 0 0 0 and the Ir at $00\frac{1}{2}$ in $I2/m$ and $\frac{1}{2}\frac{1}{2}\frac{1}{2}$ in both $R\bar{3}$ and $Fm\bar{3}m$.

[33], the fact that it is not observed in the low-temperature structure suggests this may reflect a compromise in the bonding requirements of the three cations.

The strain in the monoclinic structure is also indicated by the lattice parameters. In space group $I2/m$ (tilt system $a^-a^-c^0$) the tilting of *rigid* octahedra around a diad axis of the parent perovskite, will result in the a-axis being slightly longer than the b-axis. However, as noted by Zhou and Goodenough [34], competition between cooperative tilting and distortions of the octahedra can alter the relative magnitude of the lattice parameters and there is at least one other well characterised example of a double perovskite in $I2/m$ with $a < b$, namely Sr_2CrSb_6 [35]. Given the paucity of well characterised examples of double perovskites in $I2/m$, compared to $P2_1/n$ little importance can be placed on this observation that a is less than b in the monoclinic phase.

Cooling the sample to 100 K induced a second transition to a triclinic phase in $I\bar{1}$. The average bond distances in the triclinic phase of Ba_2LaIrO_6 at 11 K are similar to those observed at room temperature, Ir–O 1.968 and La–O 2.337 Å, although in this case the bond distance anisotropy in much less. In summary we find Ba_2LaIrO_6 to be cubic above 463 K transforming to a rhombohedral $R\bar{3}$ phase. Near 373 K a monoclinic structure in $I2/m$ appears, this becoming the major phase at room temperature. The present work resolves the decades long uncertainty regarding the actual structure of Ba_2LaIrO_6. It clearly demonstrates the importance of using high resolution neutron diffraction in establishing precise structures for cation-ordered perovskites and highlights the advantages of using variable temperatures in the study of complex perovskite structures.

Acknowledgments

BJK is grateful to the support of the Australian Research Council for this work. This work was, in part, performed at the Australian Synchrotron.

Appendix A. Supplementary materials

Supplementary data associated with this article can be found in the online version at doi:10.1016/j.jssc.2009.08.026.

References

[1] H.D. Megaw, Proceedings of the Physical Society of London 58 (1946) 133.
[2] G. Blasse, Journal of Inorganic & Nuclear Chemistry 27 (1965) 993.
[3] L. Katz, R. Ward, Inorganic Chemistry 3 (1964) 205.
[4] P.D. Battle, J.G. Gore, R.C. Hollyman, A.V. Powell, Journal of Alloys and Compounds 218 (1995) 110.
[5] J.M. Longo, P.M. Raccah, J.B. Goodenough, Journal of Applied Physics 39 (1968) 1327.
[6] Y. Maeno, H. Hashimoto, K. Yoshida, S. Nishizaki, T. Fujita, J.G. Bednorz F. Lichtenberg, Nature 372 (1994) 532.
[7] I. Thumm, U. Treiber, S. Kemmlersack, Journal of Solid State Chemistry 35 (1980) 156.
[8] E.M. Ramos, I. Alvarez, R. Saezpuche, M.L. Veiga, C. Pico, Journal of Alloys and Compounds 225 (1995) 212.
[9] M. Wakeshima, D. Harada, Y. Hinatsu, Journal of Alloys and Compounds 287 (1999) 130.
[10] W.T. Fu, D.J.W. Ijdo, Journal of Alloys and Compounds 394 (2005) L5.
[11] H.P. Xiang, X.J. Liu, X.F. Hao, J. Meng, Z.J. Wu, Journal of Alloys and Compounds 457 (2008) 571.
[12] C. Glover, J. McKinlay, M. Clift, B. Barg, A. Broadbent, J. Boldeman, M. Ridgway, G. Foran, R. Garrett, P.A. Lay, in: Fifth International Conference on Synchrotron Radiation in Materials Science, 2006, p. 282.
[13] K.S. Wallwork, B.J. Kennedy, D. Wang, AIP Conference Proceedings 879 (2007) 879.
[14] K.D. Liss, B.A. Hunter, M. Hagen, T. Noakes, S.J. Kennedy, Physica B Condensed Matter 385–386 (2006) 1010.
[15] B.A. Hunter, C.J. Howard, A Computer Program for Rietveld Analysis of X-Ray and, Lucas Heights Research Laboratories, Sydney, 1998, p. 1.
[16] J.H. Choy, D.K. Kim, S.H. Hwang, G. Demazeau, D.Y. Jung, Journal of the American Chemical Society 117 (1995) 8557.
[17] C.J. Howard, B.J. Kennedy, P.M. Woodward, Acta Crystallographica Section B—Structural Science 59 (2003) 463.
[18] Q.D. Zhou, B.J. Kennedy, Journal of Physics and Chemistry of Solids 67 (2006) 1595.
[19] C.J. Ball, B.D. Begg, D.J. Cookson, G.J. Thorogood, E.R. Vance, Journal of Solid State Chemistry 139 (1998) 238.
[20] R.C. Currie, J.F. Vente, E. Frikkee, D.J.W. Ijdo, Journal of Solid State Chemistry 116 (1995) 199.
[21] P.D. Battle, J.G. Gore, Journal of Materials Chemistry 6 (1996) 1375.
[22] P.D. Battle, J.B. Goodenough, R. Price, Journal of Solid State Chemistry 46 (1983) 234.
[23] P.J. Saines, J.R. Spencer, B.J. Kennedy, Y. Kubota, C. Minakata, H. Hano, K. Kato, M. Takata, Journal of Solid State Chemistry 180 (2007) 3001.
[24] W.T. Fu, Y.S. Au, S. Akerboom, D.J. Ijdo, Journal of Solid State Chemistry 181 (2008) 2523.
[25] A.A. Bolzan, C. Fong, B.J. Kennedy, C.J. Howard, Acta Crystallographica Section B—Structural Science 53 (1997) 373.
[26] Q.D. Zhou, B.J. Kennedy, Journal of Solid State Chemistry 178 (2005) 3589.
[27] I.D. Brown, Journal of Solid State Chemistry 90 (1991) 155.

[28] B.J. Kennedy, C.J. Howard, K.S. Knight, Z.M. Zhang, Q.D. Zhou, Acta Crystallographica Section B—Structural Science 62 (2006) 537.
[29] P.J. Saines, J.R. Spencer, B.J. Kennedy, M. Avdeev, Journal of Solid State Chemistry 180 (2007) 2991.
[30] P.J. Saines, B.J. Kennedy, M.M. Elcombe, Journal of Solid State Chemistry 180 (2007) 401.
[31] W.T. Fu, S. Akerboom, D.J.W. Ijdo, Journal of Solid State Chemistry 180 (2007) 1547.
[32] J. Rodriguez-Carvajal, M. Hennion, F. Moussa, A.H. Moudden, L. Pinsard, A. Revcolevschi, Physical Review B 57 (1998) R3189.
[33] Q.D. Zhou, B.J. Kennedy, Journal of Physics and Chemistry of Solids 68 (2007) 1643.
[34] J.S. Zhou, J.B. Goodenough, Physical Review Letters 94 (2005) 4.
[35] A. Faik, J.M. Igartua, M. Gateshki, G.J. Cuello, Journal of Solid State Chemistry 182 (2009) 1717.